

Lift Curve Breakdown for Airfoil undergoing Dynamic Stall

A. Choudhry¹, M. Arjomandi² and R. Kelso³

^{1,2,3}School of Mechanical Engineering
 University of Adelaide, South Australia 5005, Australia

Abstract

The work presented aims to investigate the lift-characteristics of a thick airfoil section undergoing dynamic stall. The NACA 0021 airfoil was selected for the experimental work performed at the KC Wind Tunnel at the University of Adelaide. The airfoil was pitched at the mid-chord and the unsteady surface pressure distributions were recorded. The surface pressures were then used to obtain the lift-curve for the airfoil undergoing dynamic stall. In the present article, the unsteady lift-curve has been broken down into stages and each stage has been analysed to gain a deeper understanding of the dynamic stall lift.

Introduction

Dynamic stall is one of the most critical factors that limits the design and operation of aerodynamic-related applications such as helicopters, MAVs and wind turbines [1-4]. It can be considered as the delay of conventional flow separation caused by a rapid increase in the angle of attack beyond the steady-state stall angle of attack. The unsteady motion results in the generation of an intense vorticity field which, in turn, results in a large increase in the airfoil lift. Due to the inherent complexity of the dynamic stall process, several theories exist in the present literature as to the cause of large increase in lift during the pitch-up motion of an airfoil. Earlier research [5-7] has shown that the primary increase in the lift is caused by the presence of the dynamic stall vortex (DSV). On the other hand, Albertson et al. [8] showed that the DSV was not responsible for the increase in lift during the entire cycle and that majority of the lift generated by the airfoil was prior to the formation of the DSV. The lack of a consensus regarding the generation of lift during unsteady pitch-up prompted the authors of the present article to undertake a thorough study of the dynamic stall process, particularly the lift.

In this article, the lift-curve of a NACA 0021 airfoil, undergoing dynamic stall, has been broken down into sub-stages and each stage has been analysed separately. Surface pressure measurements were recorded for the airfoil, being pitched at the mid-chord, to obtain the lift force. The airfoil was pitched at constant pitch rates starting from an angle of attack of zero degrees to a pre-determined maximum angle of attack, well-beyond the stall angle of attack. It was, then, allowed to maintain the maximum angle of attack for several chord lengths of flow travel. The details of the experimental procedure have been presented in the following section, followed by an in-depth analysis of the lift generated by the airfoil and the potential causes of its behaviour.

Experimental Setup

The experiments were conducted on the NACA 0021 airfoil in the closed-loop KC Wind Tunnel at the University of Adelaide, shown in Figure 1. The working section of the tunnel has a cross section of 0.5m x 0.5m and the airfoil was placed vertically in the working section at the centre. The turbulence intensity of the oncoming flow at the location of the foil was measured to be 0.6%. The test Reynolds number based on the 0.1m chord length of the airfoil was 50,000.



Figure 1. The KC Wind Tunnel used in the present experimental work indicating the setup.

The airfoil was constructed using acrylic in two parts. The pressure taps were placed along the mid-chord of the airfoil, based on a similar distribution as that used by Jumper et al [9]. The airfoil chord length was 100mm, resulting in a blockage ratio of 12% at an angle of attack of 40deg. It is important to note that dynamic blockage is of little significance, as shown by Granlund et al [10], and, therefore, no corrections were applied to the results. The total span of the airfoil was 495mm, in order to minimize the three-dimensional effects caused by the tip vortices. The airfoil was instrumented using *TruStability*[®] differential pressure sensors that were placed inside the foil. The positive port of the sensors was connected to the pressure taps using copper tubing and flexible plastic hoses. The negative ports were connected to a single reference plenum that provided the freestream static pressure. The differential measurements were recorded using the *National Instruments*[®] USB-6210 Data Acquisition System (NI-DAQ) at a rate of 5000 samples per second. The airfoil was rotated about its mid-chord using a 22mm diameter *Maxon*[®] brushed DC electric motor and an electronic position encoder to monitor the velocity and position of the airfoil. The encoder was controlled using a computer-based system through an in-house code. The surface pressures were non-dimensionalised using the dynamic pressure, measured by a Pitot-static tube, giving the pressure coefficient (C_p). The chord-normal (C_N) and chord-axial (C_A) aerodynamic force coefficients were obtained through integration of the area between the pressure distribution curves:

$$C_N = - \oint C_p d \left(\frac{x}{c} \right)$$

$$C_A = \oint C_p d \left(\frac{y}{c} \right)$$

Finally, the lift (C_L) and pressure drag (C_D) coefficients were determined using the following expressions:

$$C_L = C_N \cos \alpha - C_A \sin \alpha$$

$$C_D = C_N \sin \alpha + C_A \cos \alpha$$

Each test case was repeated ten times in order to obtain the averaged results. Furthermore, the pitch rates have been described in terms of the conventionally used reduced frequency. For an airfoil of chord length of c , pitching about the mid-chord at a constant pitch rate of $\dot{\alpha}$ (rad/s), the reduced frequency can be defined by:

$$\kappa = \frac{\dot{\alpha} c}{2U}$$

Dynamic Stall Lift Characteristics

Considerable research has been conducted in order to understand the effects of the pitch rate (reduced frequency) on the dynamic stall process for different airfoils [9, 11, 12]. It has been observed that an increase in the reduced frequency results in the delay of DSV formation to higher angles as well as a considerable increase in the lift force. A similar behaviour has been noted for the present study where the NACA 0021 airfoil was pitched at the mid-chord location at increasing reduced frequencies. The increase in the dynamic stall angle of attack and the maximum lift can clearly be observed in Figure 2.

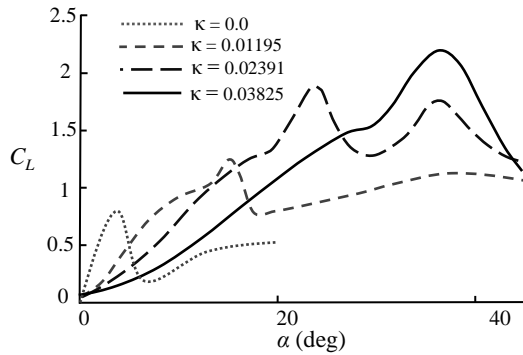


Figure 2. Dynamic stall lift characteristics as a function of reduced frequency ($Re = 50,000$) for the NACA 0021 airfoil.

Unlike the steady state case, several peculiarities can be observed in the unsteady lift curve for any airfoil undergoing the ramp-type motion. For an airfoil undergoing dynamic stall, the lift-curve can be divided into the pre- and post-stall regimes as indicated in Figure 3.

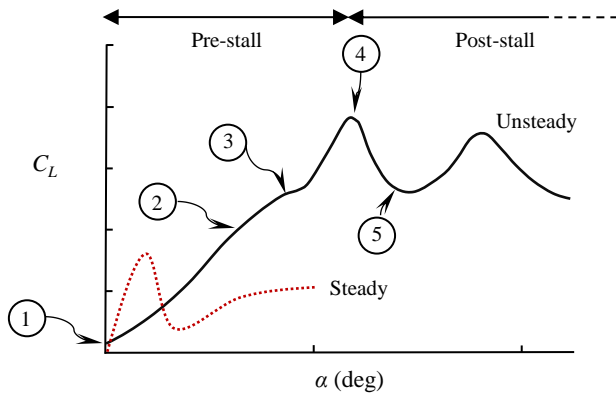


Figure 3. Schematic illustration and the stages of the lift-curve for an airfoil undergoing dynamic stall.

Furthermore, the primary lift-curve characteristics can also be identified as:

- 1: At the onset of rotation, the symmetric airfoil is observed to produce lift at an angle of attack of zero degrees.
 - 2: As the angle of attack increases, the lift curve slope starts to decrease to some extent and a slight curvature is observed in the so-called linear region of the lift curve.
 - 3: A slight kink or plateau is observed in the lift curve.
 - 4: The lift curve slope is observed to increase due to the formation of the primary DSV.
 - 5: The airfoil experiences sudden loss of lift due to complete flow separation, after the primary DSV convects.
 - 6: The airfoil continues to generate additional lift beyond the occurrence of dynamic stall due to formation of secondary vortex structures. Large-scale fluctuations in lift force are observed.
- The sub-stages involved in the pre-stall regime are investigated first, followed by the post stall regime. For the discussion, data

has been used from the current experimental campaign and other seminal works related to the field to explain the unsteady lift-characteristics of an airfoil.

The Onset

At the onset of rotation, a step increase in the lift force is observed. It was, furthermore, observed in the present study that an increase in the reduced frequency resulted in the increase of lift at the onset of rotation. The increase in lift can be explained using the Wagner's function, a quasi-steady model used to determine the lift acting at the quarter-chord ($c/4$) of the airfoil following a step change in the angle of attack. Impulsively rotating an airfoil, results in the formation of a strong vorticity near the leading edge, known as the starting vortex [13-15]. The starting vortex induces a significant amount of local velocity around the airfoil near the leading edge. However, as the vortex convects downstream, due to diffusion of its vorticity, the lift starts to decrease rapidly [16]. Due to this, the unsteady lift asymptotes towards the final steady state value. Tupper [17] proposed that the step change in lift at the onset of rotation is dependent only on the reduced frequency and the thickness-to-chord ratio of the airfoil and is given by the following expression:

$$\Delta C_L = \pi \kappa \left[1 + \frac{2}{3} (t/c) \right]$$

The above empirical approximation provides a good estimate of the step change in lift at the onset of rotation when compared with experimental observations for the NACA 0021 at a Reynolds number of 50,000 as shown in Figure 4. It can also be observed that an increase in the reduced frequency results in an approximate linear increase in the lift-step.

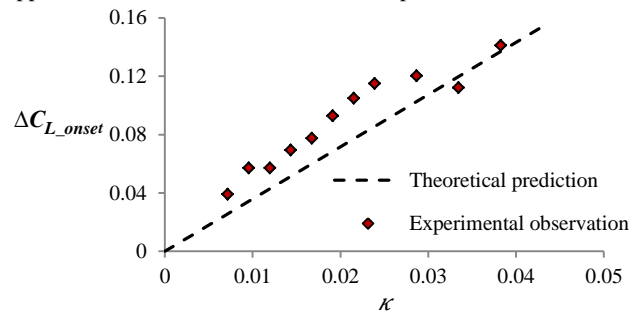


Figure 4. Comparison of theoretical lift prediction at the onset and the experimental observation for the 0021 airfoil.

The Non-Linear Lift Behaviour

After the step-increase in the lift at the onset, a continuous decrease in the lift curve slope is observed for the unsteady case as the angle of attack increases. This steady decrease eventually appears as a slight curvature in the lift slope. These changes in the lift can be attributed to the downwash caused by the pitching and can be consequently related to and predicted by the Wagner's function. In this case, a constant pitching airfoil can, therefore, be assumed to pitch in a series of steps. The unsteady increase in lift, therefore, caused by the apparent downwash of the pitching motion, tends to asymptotically approach the quasi-steady value as predicted by the Wagner's function. This results in the slight curvature observed in the lift force curve.

From a physical perspective, these phenomena can also be explained in terms of increased apparent thickness and apparent camber of the airfoil. It is well known that increasing the thickness of an airfoil results in the decrease of the lift slope, whereas, increasing the camber results in a shift of the entire lift curve upward. As observed by Jumper et al. [9], up until the quarter-chord separation (i.e. the onset of DSV formation), the general flow pattern follows the contours of the airfoil. This leads to the apparent increase in the thickness and camber as observed by the oncoming flow.

The Plateau

A plateau is observed after the non-linear part of the lift-curve. It can be argued that this is simply a continuation of the decreasing lift curve slope. However, the ‘plateau-effect’ in the lift curve is too rapid to be considered simply as the decreasing lift slope. The authors propose that the convection of the starting vortex and resultant flow reversal in the boundary layer causes the plateau in the lift curve of an airfoil undergoing unsteady motion.

Figure 5 shows the pressure distribution atop the airfoil for selected angles during the plateau-phase of the lift curve. It can be observed that the pressures gradient near the leading-edge of the airfoil is approximately zero, indicating flow separation has indeed occurred and, consequently a separation bubble is formed at the LE. Furthermore, a slight increase in the suction pressures around the quarter-chord region indicates the formation of the DSV.

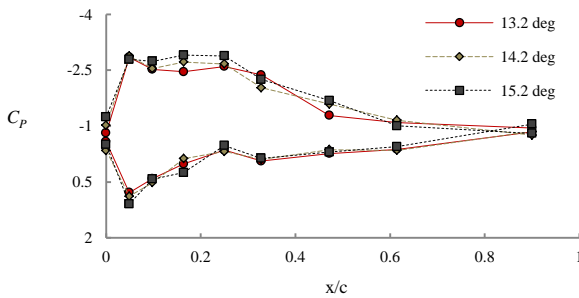


Figure 5. Pressure distribution for the NACA 0021 airfoil at angles when the lift curve has levelled off. The airfoil is pitching at $\kappa = 0.024$.

The Dynamic Stall Vortex

As the flow reversal approaches the leading edge of the airfoil, catastrophic breakdown of the separation bubble near the leading edge results in the formation of the DSV [9, 18, 19]. The presence of the DSV results in an increase of the suction pressures on the airfoil and causes the airfoil lift to increase. It can be inferred that the vortex has a low pressure core and, therefore, affects the overall lift generation during the later stages of the pitching cycle. Numerical simulations performed by Wang et al. [20] and Gharali et al. [21], for sinusoidally pitching airfoils, also illustrate the low pressure core of the vortex. Furthermore, it has been observed that an increase in the reduced frequency results in the increase in the strength of the DSV and, therefore, a higher value of maximum lift is obtained. However, the current experiments show that an indefinite increase in the reduced frequency does not seem to result in a similar increase in the maximum lift coefficient. This is illustrated in Figure 6 using a simple plot of the percentage increase in maximum lift due to dynamic stall as a function of reduced frequency for the NACA 0021 airfoil. It can be observed that after a certain reduced frequency, the lift produced by the airfoil appears to level off. Further tests are planned in order to observe the trends of maximum lift coefficient at larger reduced frequencies and Reynolds numbers.

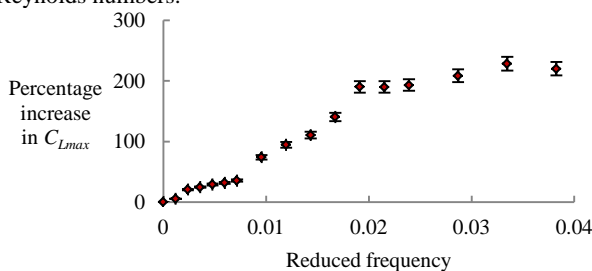


Figure 6. Percentage increase in the maximum lift as a function of reduced frequency at a Reynolds number of 50,000.

The Stall

After its inception, the DSV, under the influence of the freestream flow, convects over the surface of the airfoil inducing a complex, non-linear pressure field. As the vortex moves downstream, the forces and moments generated by the airfoil reach their respective maximum values, albeit not exactly simultaneously. Secondary and sometimes tertiary vortices are also observed occasionally and produce additional fluctuations in the aerodynamic loads, although to a greatly reduced extent as compared to the effects of the primary DSV [22]. Finally, after the DSV departs from the vicinity of the airfoil, large scale flow separation is observed. According to the definition of Sears & Telionis [23], the airfoil is now under a state of complete unsteady stall. The convection of the DSV from the airfoil surface causes a rapid decrease in the lift of the airfoil.

It is difficult to estimate the intensity of stall from simple visual inspection of the flow or direct comparison of lift curves. For this reason, the authors of the current article present a new parameter termed the stall intensity factor. The stall intensity factor for the steady-state case and the ramp-type unsteady case can be defined using the lift slope ($\Delta C_l / \Delta \alpha$) after separation and the overall decrease in lift after the first peak (ΔC_l) and prior to the secondary peak as:

$$SI = \left(\frac{\Delta C_l}{\Delta \alpha} \right) (\Delta C_l)$$

Using the definition of stall intensity factor, the stall behaviour of airfoils operating at both steady and unsteady conditions can be examined and systematically evaluated. For the dynamic stall case, the effects of increasing the reduced frequency on the stall intensity have been presented in Figure 7 for the NACA 0021 airfoil from the current experiment and the NACA 0015 airfoil from Jumper et al. [9]. Note that a reduced frequency of zero implies the steady-state case. It can be observed that an increase in the reduced frequency results in the increase of the stall intensity factor in an approximate linear fashion for both airfoils (NACA 0021 and NACA 0015). This indicates that increasing the reduced frequency, while keeping the other parameters of operation constant, results in an increase in the severity of stall experienced by the airfoil. Furthermore, the severity of stall is larger for the thicker airfoil at the smaller reduced frequencies. However, as the reduced frequency is increased, the thinner airfoil experiences a severer unsteady-stall, compared to the thicker airfoil.

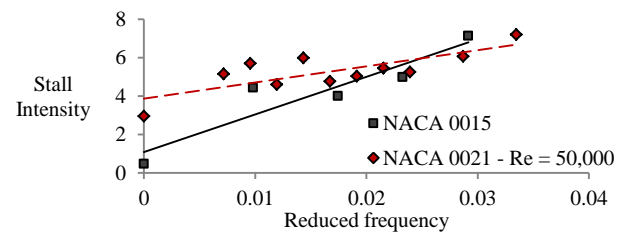


Figure 7. Effects of increasing reduced frequency on the stall intensity factor of two different airfoils (NACA 0015 from Jumper et al. (1987b) and the NACA 0021 from current experiments).

Further experiments are planned in order to understand the effects of increasing reduced frequencies and Reynolds number on the stall intensity of the airfoil.

It has been noted from earlier literature review that if the airfoil is allowed to pitch up to a maximum angle of attack of 90deg, a clear resemblance is observed with the lift behaviour of a flat plate. The aerodynamic lifting characteristics of both the airfoil and the flat plate exhibit a parabolic trend with changing angle of attack. This can be observed in Figure 8. Therefore, after dynamic stall, the airfoil starts to behave similar to a rotating flat plate, much like an airfoil behaving similar to a flat plate after simple steady-state stall. Note that here the general trend in the

behaviour of the lift curve is of particular importance since a direct comparison of both the cases is not reasonable due to the dissimilar operating conditions and the imposed unsteadiness.

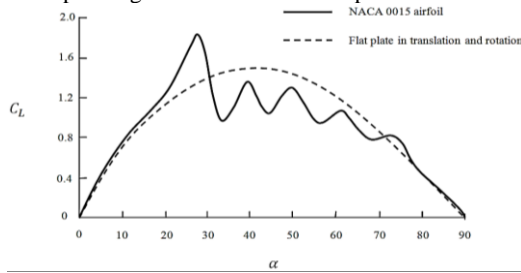


Figure 8 - Lift coefficient for a pitching 0015 airfoil [24] and a flat plate undergoing both rotation and translation [25], showing similar parabolic trend.

Conclusion

The present article presents an insight into the dynamic stall lift characteristics of an airfoil section. For this study, a NACA 0021 airfoil was pitched at its mid-chord at a Reynolds number of 50,000. The lift-curve of the airfoil was broken down into stages and each stage was analysed separately in detail to understand the cause of lift production during the dynamic stall process. The lift-curve characteristics of an airfoil pitching at constant rates can be summarized as follows:

1. At the onset of rotation, the lift produced at zero angle of attack for the unsteady case is found to be slightly larger as compared to that produced by the simple symmetric airfoil. This is primarily due to the effects of a starting vortex that induces additional circulation near the airfoil leading edge. The effects of the starting vortex can be modelled using Tupper's [17] equation.
2. As the angle of attack increases, the lift curve slope of the airfoil starts to decrease continually and a slight curvature is observed. This behaviour can be explained due to the thickening of the boundary layer on the suction side of the airfoil, resulting in apparent thickness and camber changes for the airfoil.
3. The sudden plateau observed in the lift curve can be considered as partial flow separation and can be attributed to the formation of leading-edge separation bubble.
4. After the plateau, an evident increase in the lift slope occurs for a pitching airfoil due to the formation of the DSV. Furthermore, as the reduced frequency increases, the maximum lift during the dynamic stall process also increases. However, a limiting factor to the maximum lift was observed in the current work.
5. A sudden drop in the lift is observed when the DSV detaches from the airfoil surface. The stall can be characterized using a newly-formulated parameter known as the stall intensity factor. It has been observed that the stall intensity worsens as reduced frequency is increased.

References

[1] Choudhry, A., M. Arjomandi, & R. Kelso, Horizontal axis wind turbine dynamic stall predictions based on wind speed and direction variability. *Proceedings of the Institution of Mechanical Engineers, Part A: Journal of Power and Energy*, 2013. **227**(3): p. 338-351.

[2] Laratro, A., Arjomandi M, Kelso R & Cazzolato B., A discussion of wind turbine interaction and stall contributions to wind farm noise. *Journal of Wind Engineering and Industrial Aerodynamics*, 2014. **127**: p. 1-10.

[3] Choudhry, A., M. Arjomandi, & R. Kelso, Estimation of dynamic stall on wind turbine blades using an analytical model. *18th Australasian Fluid Mechanics Conference 2012, Launceston, Tasmania*.

[4] Choudhry, A., Mo J-O, Arjomandi M & Kelso R., Effects of spacing between wind turbines on blade dynamic stall. *18th Australasian Fluid Mechanics Conference 2012, Launceston, Tasmania*.

[5] Ericson, L.E. & Reding J.P., Analytic prediction of dynamic stall characteristics. 1972: American Institute of Aeronautics and Astronautics.

[6] McCroskey, W.J., McAlister KW, Carr LW, Pucci SL, Lambert O & Indergrand RF, Dynamic stall on advanced airfoil sections. *Journal of the American Helicopter Society*, 1981. **26**(3): p. 40-50.

[7] Walker, J., Helin H., & Strickland J., An experimental investigation of an airfoil undergoing large-amplitude pitching motions. *AIAA journal*, 1985. **23**(8): p. 1141-1142.

[8] Albertson, J., Trout T, Siuru W. & Walker J., *Dynamic stall vortex development and the surface pressure field of a pitching airfoil*. 1987, DTIC Document.

[9] Jumper, E., Schreck S., & Dimmick R., Lift-curve characteristics for an airfoil pitching at constant rate. *Journal of Aircraft*, 1987. **24**: p. 680-687.

[10] Granlund, K., Ol M, Garmann D, Visbal M & Bernal L., Experiments and computations on abstractions of perching. *AIAA*, 2010. **4943**.

[11] Schreck, S.J., *Unsteady vortex dynamics and surface pressure topologies on a finite pitching wing*. 1994, DTIC Document.

[12] Rival, D. & Tropea C., Characteristics of pitching and plunging airfoils under dynamic-stall conditions. *Journal of Aircraft*, 2010. **47**(1): p. 80-86.

[13] Freymuth, P., The vortex patterns of dynamic separation: a parametric & comparative study. *Progress in Aerospace Sciences*, 1985. **22**(3): p. 161-208.

[14] Ohmi, K., Coutanceau M, Loc TP & Dulieu A, Vortex formation around an oscillating and translating airfoil at large incidences. *Journal of Fluid Mechanics*, 1990. **211**(1): p. 37-60.

[15] Panda, J. & Zaman K., Experimental investigation of the flow field of an oscillating airfoil and estimation of lift from wake surveys. *Journal of Fluid Mechanics*, 1994. **265**: p. 65-96.

[16] Mehta, U.B. & Lavan Z., Starting vortex, separation bubbles and stall: a numerical study of laminar unsteady flow around an airfoil. *Journal of Fluid Mechanics*, 1975. **67**(02): p. 227-256.

[17] Tupper, K., *The Effect of Trailing Vortices on the Production of Lift on an Airfoil Undergoing a Constant Rate of Change of Angle of Attack*. 1983, DTIC Document.

[18] McCroskey, W., Carr L., & McAlister K., Dynamic stall experiments on oscillating airfoils. *AIAA Journal*, 1976. **14**(1): p. 57-63.

[19] McAlister, K., Carr L., & McCroskey W., *Dynamic stall experiments on the NACA 0012 airfoil*. NASA-TP-1100. 1978.

[20] Wang, S., Ingham DB, Ma L, Pourkashanian M & Tao Z., Turbulence modeling of deep dynamic stall at relatively low Reynolds number. *Journal of Fluids and Structures*, 2012. **33**: p. 191-209.

[21] Gharali, K. & Johnson D.A., Dynamic stall simulation of a pitching airfoil under unsteady freestream velocity. *Journal of Fluids and Structures*, 2013.

[22] McCroskey, W., *The phenomenon of dynamic stall*. 1981, DTIC Document.

[23] Sears, W. & Telionis D., Boundary-layer separation in unsteady flow. *SIAM Journal on Applied Mathematics*, 1975. **28**(1): p. 215-235.

[24] Jumper, E., Hitchcock J., & Docken R., Investigating dynamic stall using a modified momentum-integral method. in *AIAA, Aerospace Sciences Meeting, 25 th, Reno, NV*. 1987.

[25] Dickinson, M.H. & Gotz K.G., Unsteady aerodynamic performance of model wings at low Reynolds numbers. *Journal of Experimental Biology*, 1993. **174**(1): p. 45-64.